CONDENSED MATTER PHYSICS

Ultrafast time-resolved x-ray scattering reveals diffusive charge order dynamics in $La_{2-x}Ba_xCuO_4$

Matteo Mitrano[1,2]*, Sangjun Lee[1,2], Ali A. Husain[1,2], Luca Delacretaz[3], Minhui Zhu[1], Gilberto de la Peña Munoz[4], Stella X.-L. Sun[1,2], Young Il Joe[5], Alexander H. Reid[4], Scott F. Wandel[4†], Giacomo Coslovich[4], William Schlotter[4], Tim van Driel[4], John Schneeloch[6‡], G. D. Gu[6], Sean Hartnoll[3], Nigel Goldenfeld[1]*, Peter Abbamonte[1,2]*

Charge order is universal among high-T_c cuprates, but its relation to superconductivity is unclear. While static order competes with superconductivity, dynamic order may be favorable and even contribute to Cooper pairing. Using time-resolved resonant soft x-ray scattering at a free-electron laser, we show that the charge order in prototypical $La_{2-x}Ba_xCuO_4$ exhibits transverse fluctuations at picosecond time scales. These sub–millielectron volt excitations propagate by Brownian-like diffusion and have an energy scale remarkably close to the superconducting T_c. At sub–millielectron volt energy scales, the dynamics are governed by universal scaling laws defined by the propagation of topological defects. Our results show that charge order in $La_{2-x}Ba_xCuO_4$ exhibits dynamics favorable to the in-plane superconducting tunneling and establish time-resolved x-rays as a means to study excitations at energy scales inaccessible to conventional scattering techniques.

INTRODUCTION

One of the key questions in high-temperature superconductivity is how it emerges as hole-like carriers are added to a correlated Mott insulator (*1*–*3*). Soon after the discovery of Bednorz and Müller (*4*), it was recognized that competition between kinetic energy and Coulomb repulsion could cause valence holes to segregate into periodic structures originally referred to as "stripes" (*5*–*7*). Valence band charge order has since been observed in nearly all cuprate families (*8*–*19*), although it is not known what role, if any, charge order plays in superconductivity.

It is widely believed that, while static charge order may compete with superconductivity, fluctuating order could be favorable or even contribute to the pairing mechanism (*1*, *2*, *20*). For example, transverse stripe fluctuations have been cited as a means to enhance superconductivity by modulating the interstripe Josephson coupling (*1*, *21*). It is therefore crucial to determine whether the charge order in cuprates is fluctuating and, if so, what kind of dynamics it exhibits.

The generally accepted way to detect fluctuating charge order is to use energy- and momentum-resolved scattering techniques, such as inelastic x-ray or electron scattering, to measure the dynamic structure factor, $S(q, \omega)$ (*2*, *20*). This quantity is related to the charge susceptibility, $\chi''(q, \omega)$, by the fluctuation-dissipation theorem, which asserts a quantitative relationship between the weakly nonequilibrium dynamics of a system and its equilibrium fluctuations at finite temperature (*22*–*25*). The time scale of the fluctuations can therefore be inferred from the energy dependence of the scattering data. The energy scale of charge fluctuations could, however, be of the same order as the superconducting gap, requiring instruments with sub–millielectron volt energy resolution to detect it. These x-ray and electron spectrometers do not yet exist, calling for a different approach.

An alternative way to achieve sub–millielectron volt energy resolution is to study the collective excitations in the time domain. The effective energy resolution of a time-resolved experiment can be defined as $\Delta\omega = 2\pi\hbar/t_d$, where t_d is the time interval measured (*26*). Arbitrarily low energy scales can therefore be accessed by scanning to long delay times. Furthermore, the fluctuation-dissipation theorem guarantees that the time-domain dynamics of a system may be used to shed light on its low-energy fluctuations in equilibrium.

When an ordered phase is excited out of equilibrium, its order parameter could exhibit any of several distinct types of dynamics (*23*–*25*). For example, it might exhibit inertial dynamics, undergoing coherent oscillation around its equilibrium value at a characteristic frequency. These dynamics are common in structural phase transitions in which the oscillation is a phonon of the distorted phase. Alternatively, the order parameter might relax back to equilibrium gradually, through either dissipation or diffusive motion of excitations. This relaxation is influenced by conservation laws and by the possible presence of continuous symmetries that support topological defects (*24*, *25*). Recent time-resolved optics studies of underdoped $YBa_2Cu_3O_{6+x}$ and $La_{2-x}Sr_xCuO_4$ showed coherent, millielectron volt–scale oscillations that were interpreted as an amplitude mode of the charge order (*27*–*29*), implying that the charge dynamics are inertial (*24*, *25*). However, optics experiments probe the system at zero momentum and are not selectively sensitive to charge order, which is an innately finite-momentum phenomenon. Hence, momentum-resolved techniques capable of directly studying the microscopic dynamics of the charge order are greatly needed.

RESULTS AND DISCUSSION

Here, we use time-resolved resonant soft x-ray scattering (tr-RSXS) to study the collective dynamics of "stripe-ordered" $La_{2-x}Ba_xCuO_4$ with $x \sim 1/8$ (LBCO) (*8*, *9*, *30*). We use 50-fs, 1.55-eV laser pulses to drive the charge order parameter out of equilibrium and probe its subsequent dynamics by scattering 60-fs x-ray pulses from a free-electron

[1]Department of Physics, University of Illinois at Urbana-Champaign, Urbana, IL 61801, USA. [2]Seitz Materials Research Laboratory, University of Illinois at Urbana-Champaign, Urbana, IL 61801, USA. [3]Department of Physics, Stanford University, Stanford, CA 94305-4060, USA. [4]SLAC National Accelerator Laboratory, 2575 Sand Hill Road, Menlo Park, CA 94025, USA. [5]National Institute of Standards and Technology, Boulder, CO 80305, USA. [6]Condensed Matter Physics and Materials Science Department, Brookhaven National Laboratory, Upton, NY 11973, USA.
*Corresponding author. Email: mmitrano@illinois.edu (M.M.); nigel@illinois.edu (N.G.); abbamonte@mrl.illinois.edu (P.A.)
†Present address: MIT Lincoln Laboratory, 244 Wood Street, Lexington, MA 02421, USA.
‡Present address: Department of Physics, University of Virginia, Charlottesville, VA 22904, USA.

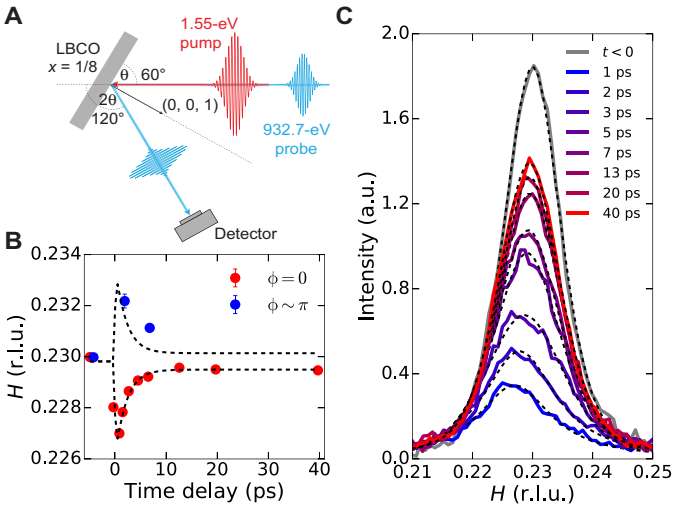

Fig. 1. Pump-induced suppression and recoil of the charge order in LBCO. (**A**) Sketch of the experiment. Pump pulses of 1.55 eV perturb the charge order, which is then probed by resonant scattering of copropagating soft x-ray FEL pulses resonantly tuned to the Cu $L_{3/2}$ edge. In this experiment, there is an additional surface miscut of 21° from the *ab* plane. (**B**) Time-dependent shift of the charge order wave vector in the *H* momentum direction for two different azimuthal sample angles, $\phi = 0$ and π. Error bars represent the SD of the pseudo-Voigt peak position fit. The dashed line is a fit to the $\phi = 0$ data (reflected for comparison to the $\phi = \pi$ points) with an exponential function of the type $H(t) = H_0 + \Theta(t)(1 - e^{-t/\tau_0})(\delta H e^{-t/\tau} + \delta H_\infty)$ (note S2). (**C**) Transverse momentum scan in the *H* direction through the charge order peak for a selection of time delays. Dashed lines are fits using a pseudo-Voigt function (note S2). The fluorescence background has been subtracted. a.u., arbitrary units.

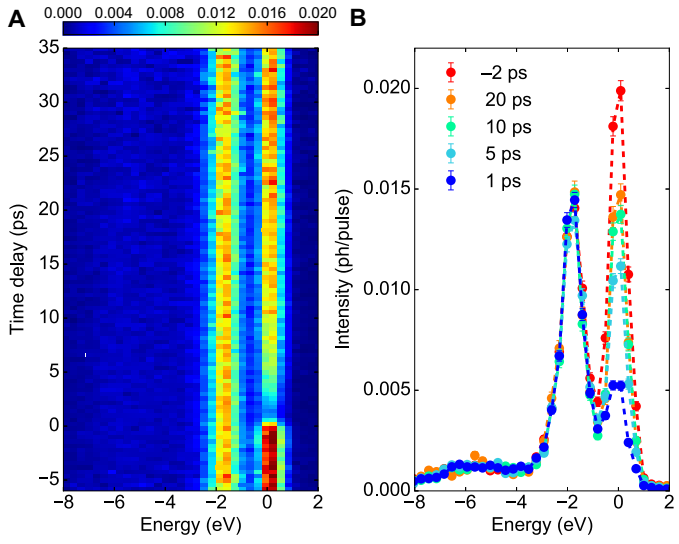

Fig. 2. tr-RIXS measurement of charge order in LBCO. (**A**) tr-RIXS spectra taken at a series of delay times, with the momentum tuned to the peak of the charge order, Q_{co} (data are binned in 400-fs time steps to reduce counting noise in the plot). (**B**) Line plots of the same tr-RIXS spectra for a selection of time delays. Error bars represent Poisson counting error. The quasi-elastic scattering from the charge order appears at zero energy and is the only spectral feature influenced by the pump. The feature at −1.8 eV is a combination of *dd* excitations and Cu^{2+} emission, and the features at −6 eV are charge transfer excitations.

laser (FEL) after a controlled time delay (Fig. 1A). X-ray pulses were resonantly tuned to the Cu $L_{3/2}$ edge (931.5 eV) and detected with either an energy-integrating avalanche photodiode (APD) or an energy-resolving soft x-ray grating spectrometer with a resolution of 0.7 eV (*31*, *32*). Using the latter makes this is a time-resolved resonant inelastic x-ray scattering (tr-RIXS) measurement and allows the isolation of the resonant, valence band scattering from the Cu^{2+} fluorescence background. A total delay range of $t_d = 40$ ps after the pump arrival was scanned with a time resolution of $\Delta t = 130$ fs (fig. S1), allowing studies of phenomena with an energy scale ranging from $2\pi\hbar/t_d = 0.103$ meV to $\pi\hbar/\Delta t = 15.9$ meV (*26*).

LBCO is considered the most charge-ordered cuprate. With a correlation length reaching hundreds of lattice parameters, its charge order is often considered "static" (*9*, *30*), making it a stringent test case for fluctuating order. Above the transition temperature T_{co}, recent scattering experiments reported evidence of precursory and possibly fluctuating charge order correlations (*33*). The crystal used here orders below $T_{CO} = 53$ K, which coincides with an orthorhombic-to-tetragonal structural transition (*8*, *9*, *30*). Experiments were carried out at $T = 12$ K, which is above the superconducting $T_c = 5$ K, and focused around the charge order wave vector $\vec{Q}_{CO} = (0.23, 0.00, 1.50)$ reciprocal lattice units (r.l.u.), where (*H*, *K*, *L*) are Miller indices denoting the location of the peak in momentum space (see Materials and Methods for further details) (*9*, *30*).

tr-RSXS directly reveals the dynamics of the charge order parameter. A transverse momentum scan through the charge order reflection at a delay time of 1 ps and a pump fluence of 0.1 mJ/cm^2 (Fig. 1C and fig. S3) shows that the peak is suppressed by 75% and broadened in momentum by 45% compared to its equilibrium value, as determined by a pseudo-Voigt fit (note S2) (*34*–*36*). That the peak is not fully suppressed implies that the laser provided a perturbation of intermediate strength, with which the charge order is not fully extinguished. The broadening of the peak indicates the creation of microscopic heterogeneous structure in the charge order that is transverse in character.

It is crucial to establish whether the peak changes observed are truly properties of the valence band. Repeating the measurement using energy-resolved tr-RIXS with a resolution of 0.7 eV, we find that the peak suppression only takes place in the resonant, quasi-elastic scattering (Fig. 2). The other RIXS features, including the *dd* and charge transfer excitations and Cu^{2+} fluorescence emission, are unaffected by the pump. We conclude that the effects observed are properties of the valence band and that the time response will directly reveal the dynamics of the charge order.

Shortly after the pump, for time $t \lesssim 2$ ps that corresponds to an energy scale of 2 meV $\lesssim \omega \lesssim$ 15.9 meV, we observe a shift in the wave vector of the charge order peak (see Fig. 1C). This shift occurs in the scattering plane, along the *H* momentum direction but not along the perpendicular *K* direction (fig. S2B). A single exponential fit to the time dependence (Fig. 1B) indicates that the peak position recovers in (2.13 ± 0.18) ps. This pump-induced phenomenon could be due to any of three effects: (i) a change in the periodicity of the charge order; (ii) a change in the refractive index of the sample in the soft x-ray regime, which would alter the perceived Bragg angle of the reflection (*37*); or (iii) a collective recoil of the charge order condensate.

We tested the first possibility by rotating the sample azimuthal angle by 180° and repeating the measurement at the same $\vec{Q}_{CO} = (0.23, 0.00, 1.50)$ r.l.u. If the shift were due to a periodicity change, because the CuO_2 plane is C_4 symmetric, then such a rotation would not affect the peak momentum as measured in the reference frame

of the sample. Unexpectedly, we found that the momentum shift reversed direction (Fig. 1B), meaning that it is fixed with respect to the propagation direction of the pump but not the crystal axes. This excludes a (pure) change in the periodicity of the charge order. To test the second possibility, we measured the (0, 0, 1) Bragg reflection of the low-temperature tetragonal structure. A pump-induced change in the refractive index should be visible as a shift in the (0, 0, 1) peak as well; however, no such shift was observed (fig. S6). We are led to the unexpected conclusion that the pump induces a coherent recoil of the charge order condensate—in essence, a nonequilibrium population of collective modes exhibiting a nonzero center-of-mass momentum, which might be thought of as a classical Doppler shift.

After a delay time of 2 ps, the charge order begins to recover. The next stage in its approach to equilibrium is summarized in Fig. 3A, which shows the energy-integrated intensity of the charge order peak for times 2 ps $\lesssim t \lesssim$ 10 ps, corresponding to an energy scale of 0.4 meV $\lesssim \omega \lesssim$ 2 meV. Unlike previous reports of a gapped amplitude mode (*27*–*29*), the recovery of the order parameter is purely exponential, lacking observable oscillations that would indicate inertial dynamics. This observation is unexpected because a conventional charge density wave (CDW) is normally gapped either by the crystal lattice or by disorder, resulting in inertial dynamics (*38*–*40*). It also is at odds with evidence from previous optics experiments that do not directly probe the charge order parameter (*27*–*29*). We conclude that the transverse dynamics in LBCO, previously thought to exhibit static charge order, are relaxational, meaning that the transverse excitations are gapless and will fluctuate at any finite temperature.

The momentum dependence of the charge order dynamics reveals that the collective excitations propagate by Brownian diffusion. In the standard description of relaxational dynamics in a periodic system (note S7) (*24*, *25*, *41*–*44*), a nonconserved order parameter driven weakly out of equilibrium will have a time dependence proportional to exp[−γ(*q*)*t*], where $q = |\vec{Q} - \vec{Q}_{CO}|$ is the momentum relative to the charge order peak and

$$\gamma(q) = \gamma_0 + Dq^2 \quad (1)$$

Here, γ_0 describes pure dissipation, and the momentum dependence arises from diffusion quantified by the parameter, *D*. Figure 3A shows time traces of the charge order peak intensity for $t < 10$ ps and for a selection of momenta $\vec{Q}$ along the transverse direction around $\vec{Q}_{CO}$. Each curve is fit well by a single exponential function and a constant offset that likely arises from heating of the electronic subsystem (note S6) (*45*). The exponential behavior is consistent with the charge order deviating only slightly from its equilibrium value (*24*, *25*). We find that the relaxation rate is highly momentum dependent, increasing rapidly with *q* (Fig. 3B), and is fit well by Eq. 1, yielding dissipation parameter $\hbar\gamma_0 = (0.1730 \pm 0.0015)$ meV and diffusion constant $\hbar D = (215 \pm 19)$ meV Å^2. These two quantities imply that the transverse collective excitations of the charge order in LBCO propagate by diffusion, with a characteristic diffusion length $\lambda = \sqrt{2D/\gamma_0} = (49.9 \pm 2.2)$ Å and dissipation time $1/\gamma_0 = (3.805 \pm 0.031)$ ps. Notably, the characteristic charge order fluctuation energy $\gamma_0 \sim 2$ K is similar to the superconducting T_c at $x \sim 1/8$, thus suggesting a connection between the two phenomena.

At late times, 5 ps $\lesssim t \lesssim$ 40 ps, corresponding to an energy scale of 0.1 meV $\lesssim \omega \lesssim$ 0.8 meV, the order parameter amplitude is close to its equilibrium value. The dynamics no longer follow a simple exponential function but instead are characterized by self-similar dynamic scaling (*46*–*49*). The concept of dynamic scaling originated in the field of far-from-equilibrium phenomena having been observed in phase-ordering dynamics of quenched binary fluids and alloys (*50*, *51*). The hypothesis states that the amplitude and length scale of the order parameter satisfy a universal relationship

$$S(q, t) = L^d(t)F[qL(t)] \quad (2)$$

Here, $S(q, t)$ is the time Fourier transform of $S(q, \omega)$, $L(t)$ is the characteristic length scale of the order, and $F(x)$ is a universal function. For systems with a scalar order parameter, *L* corresponds to the mean domain size. For systems with a continuous symmetry and a vector or tensor order parameter, $L(t)$ corresponds to the mean distance between topological defects and increases as defects annihilate or are annealed from the system. Equation 2 states that the fluctuations are self-similar and independent of time if suitably scaled. Dynamic scaling only takes place at late times following a quench when the magnitude of the order parameter is large and nonlinear effects are important (*47*, *52*).

Using Eq. 2, the late-time data collapse to a single curve (Fig. 4A) when taking $d = 3$ and defining $L(t)$ as the inverse of the half-width of the charge order reflection. This collapse implies that, at sub–millielectron volt energy scales, the transverse dynamics of the order parameter are determined by universal properties such as dimensionality and ranges of the interactions and are not governed by the microscopic details of LBCO itself.

The behavior of $L(t)$ is sensitive to the nature of the equilibrium phase that the system is approaching. If relaxing to a phase that is uniform in space, then $L(t)$ is known to exhibit power law behavior at

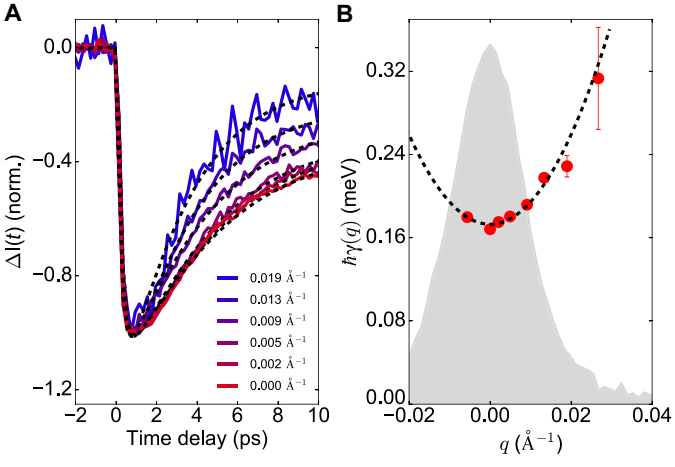

Fig. 3. Collective modes of charge order in LBCO propagate diffusively. (**A**) Solid lines: Time traces of the energy-integrated charge order scattering for a selection of momenta $q = |\vec{Q} - \vec{Q}_{CO}|$. The data are scaled to the same height and binned into 200-fs time steps to reduce counting noise in the plot. Dashed lines: Fits using a single exponential function (see note S6) show that the recovery time is highly momentum dependent. (**B**) Red points: Exponential decay parameter, γ(*q*), as a function of relative momentum difference, $q = \mathrm{sgn}(H - H_{CO})|\vec{Q} - \vec{Q}_{CO}|$. Error bars represent only the statistical uncertainties in the fits. Dashed line: Fit to the data using Eq. 1. Shaded area: Line shape of the unperturbed charge order reflection in equilibrium.

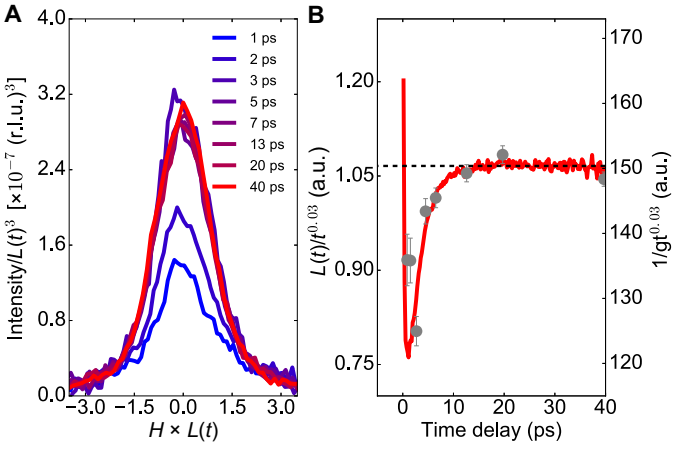

Fig. 4. Demonstration of dynamic scale invariance at long times. (**A**) Scaled momentum profiles (as in Fig. 1C) showing that the data collapse at late times for $d = 3$. Here, $L(t)$ is taken to be the inverse half-width of the reflection at each time delay, t. The curves have been shifted in H to compensate for the momentum recoil at short times. (**B**) Compensated plot of the scaling function, $L(t)$, taken to be the inverse half-width $1/g$ of the order parameter reflection (gray circles) or the cube root of the peak intensity at each time delay, t, i.e., by inverting the dynamical scaling relation $S(0, t) = L^3(t)F(0)$ (red line). The data show a power law of 0.03 at long times, indicating a logarithmic behavior.

long times, $L(t) \sim t^{\alpha}$, where $\alpha = 1/3$ if the order parameter is conserved and $\alpha = 1/2$ if it is not (*46*, *47*). If the equilibrium phase is modulated, as is the current case of charge order in LBCO, it was predicted (for a strong quench) that the long-time behavior of two-dimensional (2D) modulated phase order is governed by the dynamics of topological defects, and $L(t) \sim \ln(t)$ (*53*). These slow dynamics can arise without needing to consider additional effects due to pinning by disorder. That neighboring layers are correlated means that the topological defects behave as line defects oriented along the stacking direction and so can be described by an effective 2D dynamics.

We test these expectations by examining the long-time ($t > 10$ ps) behavior of $L(t)$. Figure 4B shows a compensated plot seemingly indicating that $L(t) \sim t^{0.03}$ at long times. Small power laws of this sort are normally interpreted as logarithmic dependence, i.e., $L(t) \sim \ln(t)$, supporting the prediction of Hou *et al.* (*53*). While disorder may be playing some role, this result is evidence that the long-time dynamics of LBCO are governed by the propagation of a dilute concentration of topological defects that are transverse in nature, such as dislocation lines. The functional form of the thermalization process of the charge-ordered phase, characterized by the presence of dynamical scaling phenomena and of diffusive behavior, is independent of the sample temperature well below the critical point.

CONCLUSION

Our results show that the charge order in LBCO is dynamic, undergoing transverse fluctuations at millielectron volt energy scales. On an energy scale of 0.4 to 2 meV, the dynamics are relaxational, meaning that the collective excitations are gapless and propagate by diffusion. This conclusion is based on the direct measurement of the charge order parameter. The gapless nature of the charge order is unexpected because a conventional CDW is normally gapped by pinning on the lattice (e.g., to the LBCO low-temperature tetragonal distortion) or impurities (*38*–*40*, *54*) and suggests that these fluctuations are a previously unidentified property specific to the cuprates. The energy scale of the transverse fluctuations is comparable to the superconducting energy, $k_B T_c$, suggesting a connection to superconductivity and supporting arguments that transverse stripe fluctuations might modulate the interstripe Josephson coupling (*1*). At ultralow-energy scales, <0.4 meV, the charge order exhibits dynamic critical scaling, indicating that the dynamics are determined by the universal propagation of transverse topological defects (*53*), e.g., dislocations in the charge order. Our study establishes tr-RSXS as a new tool to study collective charge dynamics of quantum materials at yet unexplored low-energy scales.

MATERIALS AND METHODS

Sample growth and characterization

A high-quality pellet of $La_{1.875}Ba_{0.125}CuO_4$ was grown by the floating zone method and cut into smaller single crystals (*30*). The crystals were cleaved in air to expose a fresh surface, mainly oriented along the *ab* plane. The 2-mm-sized single crystal used in this study was preoriented using a laboratory-based Cu$K\alpha$ x-ray source. The lattice parameters were determined to be $a = b = 3.787$ Å and $c = 13.23$ Å. The surface miscut with respect to the *ab* crystalline plane was found to be 21°. The superconducting T_c of the sample was verified through a SQUID (superconducting quantum interference device) magnetometry measurement to be approximately 5 K.

Time-resolved resonant soft x-ray scattering

Low-temperature optical pump, soft x-ray probe measurements were performed at the Soft X-Ray (SXR) instrument of the Linac Coherent Light Source (LCLS) X-ray FEL at SLAC National Laboratory, Menlo Park, USA (*55*). The measurements reported in this work were carried out at an RSXS endstation (*31*) in a vacuum of 3×10^{-9} torr. Low temperatures down to 12 K were achieved with a manipulator equipped with a Helium flow cryostat. Ultrafast probe x-rays at a repetition rate of 120 Hz were obtained by tuning the FEL to the Cu $L_{3/2}$ edge (931.5 eV) and with a bandwidth of 0.3 eV after passing through a grating monochromator. The p-polarized x-ray pulses had a typical pulse duration of 60 fs and a pulse energy of 1.5 μJ and were focused down to an elliptical spot of 1.5×0.03 mm^2. The optical pump pulses of 1.55 eV, also p-polarized, were generated with a Ti:sapphire amplifier run at 120 Hz and propagated collinearly with the x-rays into the RSXS endstation. The 50-fs pump was focused down to a spot of 2.0×1.0 mm^2 to probe a homogeneously excited sample volume. The beams were spatially overlapped onto a frosted Ce:YAG crystal and synchronized by monitoring the reflectivity changes of a Si_3N_4 thin film. The shot-to-shot temporal jitter between pump and probe pulses was measured by means of a timing tool (*56*, *57*) and corrected by time sorting during the data analysis. The overall time resolution of approximately 130 fs was checked by measuring the cross-correlation signal on a polished Ce:YAG crystal (see fig. S1). Shot-to-shot intensity fluctuations from the FEL were corrected in the photodiode data through a reference intensity readout before the monochromator. The scattered x-rays were measured with an energy-integrating APD located on a rotating arm at 17.3 cm from the sample, while tr-RIXS measurements were performed with a modular qRIXS grating spectrometer (*32*) mounted on a port at 135° with respect to the incident beam and provided an energy resolution of ~0.7 eV (full width at half maximum) when using the second order of the grating. The spectrometer was equipped with an ANDOR charge-coupled device camera operated at a readout rate of 120 Hz in 1D binning mode along the nondispersive direction. The

pump-probe time delay was controlled both electronically and through a mechanical translation stage. All the time-dependent rocking curves presented in this work were referenced to their equilibrium values by selectively varying the pump-probe time delay to negative values during the data acquisition to minimize errors due to motor backlash and step accuracy.

SUPPLEMENTARY MATERIALS

Supplementary material for this article is available at http://advances.sciencemag.org/cgi/content/full/5/8/eaax3346/DC1

Note S1. Pump-probe cross-correlation
Note S2. Charge order peak rocking curves fit and background subtraction
Note S3. Charge order peak rocking curves for $\phi \sim \pi$
Note S4. Comparison between tr-RIXS and APD data
Note S5. Response of the low-temperature tetragonal distortion peak
Note S6. Raw time-dependent, energy-integrated peak intensities around Q_{CO}
Note S7. Momentum-dependent recovery of the charge-ordered phase
Fig. S1. Optical pump x-ray probe cross-correlation.
Fig. S2. Pump-induced CO peak melting.
Fig. S3. Time-dependent CO peak fit parameters.
Fig. S4. CO peak shift at $\phi \sim \pi$.
Fig. S5. Comparison between tr-RIXS and energy-integrated time dependence at Q_{co}.
Fig. S6. Dynamics of the low-temperature tetragonal distortion.
Fig. S7. Raw time-dependent CO peak intensity.
Fig. S8. Schematic representation of the scattering geometry.
Table S1. Fit parameters along *K* projection.

REFERENCES AND NOTES

1. S. A. Kivelson, E. Fradkin, V. J. Emery, Electronic liquid-crystal phases of a doped mott insulator. *Nature* **393**, 550–553 (1998).
2. M. Vojta, Lattice symmetry breaking in cuprate superconductors: Stripes, nematics, and superconductivity. *Adv. Phys.* **58**, 699–820 (2009).
3. B. Keimer, S. A. Kivelson, M. R. Norman, S. Uchida, J. Zaanen, From quantum matter to high-temperature superconductivity in copper oxides. *Nature* **518**, 179–186 (2015).
4. J. G. Bednorz, K. A. Müller, Possible high T_c superconductivity in the Ba–La–Cu–O system. *Z. Phys. B: Condens. Matter* **64**, 189–193 (1986).
5. K. Machida, Magnetism in La_2CuO_4 based compounds. *Physica C* **158**, 192–196 (1989).
6. H. J. Schulz, Domain walls in a doped antiferromagnet. *J. Phys. France* **50**, 2833–2849 (1989).
7. J. Zaanen, O. Gunnarsson, Charged magnetic domain lines and the magnetism in high-T_c oxides. *Phys. Rev. B* **40**, R7391–R7394 (1989).
8. J. M. Tranquada, H. Woo, T. G. Perring, H. Goka, G. D. Gu, G. Xu, M. Fujita, K. Yamada, Quantum magnetic excitations from stripes in copper oxide superconductors. *Nature* **429**, 534–538 (2004).
9. P. Abbamonte, A. Rusydi, S. Smadici, G. D. Gu, G. A. Sawatzky, D. L. Feng, Spatially modulated 'Mottness' in $La_{2-x}Ba_xCuO_4$. *Nat. Phys.* **1**, 155–158 (2005).
10. S. A. Kivelson, E. Fradkin, *Handbook of High-Temperature Superconductivity*, J. R. Schrieffer, J. S. Brooks, Eds. (Springer Science, 2007), chap. 15, pp. 570–592.
11. G. Ghiringhelli, M. Le Tacon, M. Minola, S. Blanco-Canosa, C. Mazzoli, N. B. Brookes, G. M. De Luca, A. Frano, D. G. Hawthorn, F. He, T. Loew, M. M. Sala, D. C. Peets, M. Salluzzo, E. Schierle, R. Sutarto, G. A. Sawatzky, E. Weschke, B. Keimer, L. Braicovich, Long-range incommensurate charge fluctuations in $(Y,Nd)Ba_2Cu_3O_{6+x}$. *Science* **337**, 821–825 (2012).
12. R. Comin, A. Frano, M. M. Yee, Y. Yoshida, H. Eisaki, E. Schierle, E. Weschke, R. Sutarto, F. He, A. Soumyanarayanan, Y. He, M. Le Tacon, I. S. Elfimov, J. E. Hoffman, G. A. Sawatzky, B. Keimer, A. Damascelli, Charge order driven by Fermi-arc instability in $Bi_2Sr_{2-x}La_xCuO_{6+\delta}$. *Science* **343**, 390–392 (2014).
13. E. H. da Silva Neto, P. Aynajian, A. Frano, R. Comin, E. Schierle, E. Weschke, A. Gyenis, J. Wen, J. Schneeloch, Z. Xu, S. Ono, G. Gu, M. Le Tacon, A. Yazdani, Ubiquitous interplay between charge ordering and high-temperature superconductivity in cuprates. *Science* **343**, 393–396 (2014).
14. M. Le Tacon, A. Bosak, S. M. Souliou, G. Dellea, T. Loew, R. Heid, K.-P. Bohnen, G. Ghiringhelli, M. Krisch, B. Keimer, Inelastic x-ray scattering in $YBa_2Cu_3O_{6.6}$ reveals giant phonon anomalies and elastic central peak due to charge-density-wave formation. *Nat. Phys.* **10**, 52–58 (2014).
15. J. Chang, E. Blackburn, A. T. Holmes, N. B. Christensen, J. Larsen, J. Mesot, R. Liang, D. A. Bonn, W. N. Hardy, A. Watenphul, M. von Zimmermann, E. M. Forgan, S. M. Hayden, Direct observation of competition between superconductivity and charge density wave order in $YBa_2Cu_3O_{6.67}$. *Nat. Phys.* **8**, 871–876 (2012).
16. E. Berg, E. Fradkin, S. A. Kivelson, Theory of the striped superconductor. *Phys. Rev. B* **79**, 064515 (2009).
17. E. Fradkin, S. A. Kivelson, J. M. Tranquada, *Colloquium*: Theory of intertwined orders in high temperature superconductors. *Rev. Mod. Phys.* **87**, 457–482 (2015).
18. S. Gerber, H. Jang, H. Nojiri, S. Matsuzawa, H. Yasumura, D. A. Bonn, R. Liang, W. N. Hardy, Z. Islam, A. Mehta, S. Song, M. Sikorski, D. Stefanescu, Y. Feng, S. A. Kivelson, T. P. Devereaux, Z.-X. Shen, C. C. Kao, W. S. Lee, D. Zhu, J. S. Lee, Three-dimensional charge density wave order in $YBa_2Cu_3O_{6.67}$ at high magnetic fields. *Science* **350**, 949–952 (2015).
19. M. H. Hamidian, S. D. Edkins, S. H. Joo, A. Kostin, H. Eisaki, S. Uchida, M. J. Lawler, E. A. Kim, A. P. Mackenzie, K. Fujita, J. Lee, J. C. S. Davis, Detection of a Cooper-pair density wave in $Bi_2Sr_2CaCu_2O_{8+x}$. *Nature* **532**, 343–347 (2016).
20. S. A. Kivelson, I. P. Bindloss, E. Fradkin, V. Oganesyan, J. M. Tranquada, A. Kapitulnik, C. Howald, How to detect fluctuating stripes in the high-temperature superconductors. *Rev. Mod. Phys.* **75**, 1201–1241 (2003).
21. E. Berg, E. Fradkin, E.-A. Kim, S. A. Kivelson, V. Oganesyan, J. M. Tranquada, S. C. Zhang, Dynamical layer decoupling in a stripe-ordered high-T_c superconductor. *Phys. Rev. Lett.* **99**, 127003 (2007).
22. D. Pines, P. Noziéres, *The Theory of Quantum Liquids*, *Advanced Book Classics* (Perseus Books, 1966).
23. L. D. Landau, E. M. Lifshitz, *Physical Kinetics*, *Course of Theoretical Physics* (Pergamon Press Ltd., 1981).
24. N. Goldenfeld, *Lectures on Phase Transitions and the Renormalization Group*, *Frontiers in Physics* (Westview Press, 1992).
25. P. M. Chaikin, T. C. Lubensky, *Principles of Condensed Matter Physics* (Cambridge University Press, 1995).
26. P. Abbamonte, T. Graber, J. P. Reed, S. Smadici, C.-L. Yeh, A. Shukla, J.-P. Rueff, W. Ku, Dynamical reconstruction of the exciton in LiF with inelastic x-ray scattering. *Proc. Natl. Acad. Sci. U.S.A.* **105**, 12159–12163 (2008).
27. D. H. Torchinsky, F. Mahmood, A. T. Bollinger, I. Božović, N. Gedik, Fluctuating charge-density waves in a cuprate superconductor. *Nat. Mater.* **12**, 387–391 (2013).
28. G. L. Dakovski, W.-S. Lee, D. G. Hawthorn, N. Garner, D. Bonn, W. Hardy, R. Liang, M. C. Hoffmann, J. J. Turner, Enhanced coherent oscillations in the superconducting state of underdoped $YBa_2Cu_3O_{6+x}$ induced via ultrafast terahertz excitation. *Phys. Rev. B* **91**, 220506 (2015).
29. J. P. Hinton, J. D. Koralek, Y. M. Lu, A. Vishwanath, J. Orenstein, D. A. Bonn, W. N. Hardy, R. Liang, New collective mode in $YBa_2Cu_3O_{6+x}$ observed by time-domain reflectometry. *Phys. Rev. B* **88**, 060508 (2013).
30. M. Hücker, M. von Zimmermann, G. D. Gu, Z. J. Xu, J. S. Wen, G. Xu, H. J. Kang, A. Zheludev, J. M. Tranquada, Stripe order in superconducting $La_{2-x}Ba_xCuO_4$ ($0.095 \leq x \leq 0.155$). *Phys. Rev. B* **83**, 104506 (2011).
31. D. Doering, Y.-D. Chuang, N. Andresen, K. Chow, D. Contarato, C. Cummings, E. Domning, J. Joseph, J. S. Pepper, B. Smith, G. Zizka, C. Ford, W. S. Lee, M. Weaver, L. Patthey, J. Weizeorick, Z. Hussain, P. Denes, Development of a compact fast CCD camera and resonant soft x-ray scattering endstation for time-resolved pump-probe experiments. *Rev. Sci. Instrum.* **82**, 073303–073309 (2011).
32. Y. D. Chuang, Y. C. Shao, A. Cruz, K. Hanzel, A. Brown, A. Frano, R. Qiao, B. Smith, E. Domning, S. W. Huang, L. A. Wray, W. S. Lee, Z.-X. Shen, T. P. Devereaux, J.-W. Chiou, W.-F. Pong, V. V. Yashchuk, E. Gullikson, R. Reininger, W. Yang, J. Guo, R. Duarte, Z. Hussain, Modular soft x-ray spectrometer for applications in energy sciences and quantum materials. *Rev. Sci. Instrum.* **88**, 013110 (2017).
33. H. Miao, J. Lorenzana, G. Seibold, Y. Y. Peng, A. Amorese, F. Yakhou-Harris, K. Kummer, N. B. Brookes, R. M. Konik, V. Thampy, G. D. Gu, G. Ghiringhelli, L. Braicovich, M. P. M. Dean, High-temperature charge density wave correlations in $La_{1.875}Ba_{0.125}CuO_4$ without spin-charge locking. *Proc. Natl. Acad. Sci. U.S.A.* **114**, 12430–12435 (2017).
34. M. Först, R. I. Tobey, H. Bromberger, S. B. Wilkins, V. Khanna, A. D. Caviglia, Y. D. Chuang, W. S. Lee, W. F. Schlotter, J. J. Turner, M. P. Minitti, O. Krupin, Z. J. Xu, J. S. Wen, G. D. Gu, S. S. Dhesi, A. Cavalleri, J. P. Hill, Melting of charge stripes in vibrationally driven $La_{1.875}Ba_{0.125}CuO_4$: Assessing the respective roles of electronic and lattice order in frustrated superconductors. *Phys. Rev. Lett.* **112**, 157002 (2014).
35. V. Khanna, R. Mankowsky, M. Petrich, H. Bromberger, S. A. Cavill, E. Möhr-Vorobeva, D. Nicoletti, Y. Laplace, G. D. Gu, J. P. Hill, M. Först, A. Cavalleri, S. S. Dhesi, Restoring interlayer josephson coupling in $La_{1.885}Ba_{0.115}CuO_4$ by charge transfer melting of stripe order. *Phys. Rev. B* **93**, 224522 (2016).
36. W. S. Lee, Y. D. Chuang, R. G. Moore, Y. Zhu, L. Patthey, M. Trigo, D. H. Lu, P. S. Kirchmann, O. Krupin, M. Yi, M. Langner, N. Huse, J. S. Robinson, Y. Chen, S. Y. Zhou, G. Coslovich, B. Huber, D. A. Reis, R. A. Kaindl, R. W. Schoenlein, D. Doering, P. Denes, W. F. Schlotter, J. J. Turner, S. L. Johnson, M. Först, T. Sasagawa, Y. F. Kung, A. P. Sorini, A. F. Kemper, B. Moritz, T. P. Devereaux, D.-H. Lee, Z.-X. Shen, Z. Hussain, Phase fluctuations and the absence of topological defects in a photo-excited charge-ordered nickelate. *Nat. Commun.* **3**, 838 (2012).
37. S. Smadici, J. C. T. Lee, G. Logvenov, I. Bozovic, P. Abbamonte, Form factor dispersion at La $M_{5,4}$ edges and average density of resonant atoms. *J. Phys. Condens. Matter* **26**, 025303 (2013).

38. T. Huber, S. O. Mariager, A. Ferrer, H. Schäfer, J. A. Johnson, S. Grübel, A. Lübcke, L. Huber, T. Kubacka, C. C. Dornes, C. Laulhe, S. Ravy, G. Ingold, P. Beaud, J. Demsar, S. L. Johnson, Coherent structural dynamics of a prototypical charge-density-wave-to-metal transition. *Phys. Rev. Lett.* **113**, 026401 (2014).
39. P. Beaud, A. Caviezel, S. O. Mariager, L. Rettig, G. Ingold, C. Dornes, S.-W. Huang, J. A. Johnson, M. Radovic, T. Huber, T. Kubacka, A. Ferrer, H. T. Lemke, M. M. Chollet, D. Zhu, J. M. Glownia, M. Sikorski, A. Robert, H. Wadati, M. Nakamura, M. Kawasaki, Y. Tokura, S. L. Johnson, U. U. Staub, A time-dependent order parameter for ultrafast photoinduced phase transitions. *Nat. Mater.* **13**, 923–927 (2014).
40. G. Grüner, *Density Waves in Solids, Frontiers in Physics* (Perseus Books, 1994).
41. J. Swift, P. C. Hohenberg, Hydrodynamic fluctuations at the convective instability. *Phys. Rev. A* **15**, 319–328 (1977).
42. M. Cross, P. Hohenberg, Pattern formation outside of equilibrium. *Rev. Mod. Phys.* **65**, 851–1112 (1993).
43. M. Karttunen, M. Haataja, K. Elder, M. Grant, Defects, order, and hysteresis in driven charge-density waves. *Phys. Rev. Lett.* **83**, 3518–3521 (1999).
44. A. Newell, J. Whitehead, Finite bandwidth, finite amplitude convection. *J. Fluid Mech.* **38**, 279–303 (1969).
45. L. Perfetti, P. A. Loukakos, M. Lisowski, U. Bovensiepen, H. Eisaki, M. Wolf, Ultrafast electron relaxation in superconducting $Bi_2Sr_2CaCu_2O_{8+\delta}$ by time-resolved photoelectron spectroscopy. *Phys. Rev. Lett.* **99**, 197001 (2007).
46. A. J. Bray, Theory of phase ordering kinetics. *Adv. Phys.* **43**, 357 (1994).
47. M. Mondello, N. D. Goldenfeld, Scaling and vortex dynamics after the quench of a system with a continuous symmetry. *Phys. Rev. A* **42**, 5865–5872 (1990).
48. M. Mondello, N. D. Goldenfeld, Scaling and vortex-string dynamics in a three-dimensional system with a continuous symmetry. *Phys. Rev. A* **45**, 657–664 (1992).
49. S. Vogelgesang, G. Storeck, J. G. Horstmann, T. Diekmann, M. Sivis, S. Schramm, K. Rossnagel, S. Schäfer, C. Ropers, Phase ordering of charge density waves traced by ultrafast low-energy electron diffraction. *Nat. Phys.* **14**, 184–190 (2018).
50. Y. C. Chou, I. Goldburg, Angular distribution of light scattered from critically quenched liquid mixtures. *Phys. Rev. A* **23**, 858–864 (1981).
51. B. D. Gaulin, S. Spooner, Y. Morii, Kinetics of phase separation in $Mn_{0.67}Cu_{0.33}$. *Phys. Rev. Lett.* **59**, 668–671 (1987).
52. T. Nagaya, H. Orihara, Y. Ishibashi, Coarsening dynamics of +1 and -1 disclinations in two-dimensionally aligned nematics –spatial distribution of disclinations. *J. Physical Soc. Japan* **64**, 78–85 (1995).
53. Q. Hou, S. Sasa, N. Goldenfeld, Dynamical scaling behavior of the swift-hohenberg equation following a quench to the modulated state. *Physica A: Stat. Mech. Appl.* **239**, 219–226 (1997).
54. X. M. Chen, C. Mazzoli, Y. Cao, V. Thampy, A. M. Barbour, W. Hu, M. Lu, T. A. Assefa, H. Miao, G. Fabbris, G. D. Gu, J. M. Tranquada, M. P. M. Dean, S. B. Wilkins, I. K. Robinson, Charge density wave memory in a cuprate superconductor. *Nat. Commun.* **10**, 1435 (2019).
55. W. F. Schlotter, J. J. Turner, M. Rowen, P. Heimann, M. Holmes, O. Krupin, M. Messerschmidt, S. Moeller, J. Krzywinski, R. Soufli, M. Fernández-Perea, N. Kelez, S. Lee, R. Coffee, G. Hays, M. Beye, N. Gerken, F. Sorgenfrei, S. Hau-Riege, L. Juha, J. Chalupsky, V. Hajkova, A. P. Mancuso, A. Singer, O. Yefanov, I. A. Vartanyants, G. Cadenazzi, B. Abbey, K. A. Nugent, H. Sinn, J. Lüning, S. Schaffert, S. Eisebitt, W. S. Lee, A. Scherz, A. R. Nilsson, W. Wurth, The soft x-ray instrument for materials studies at the Linac Coherent Light Source x-ray free-electron laser. *Rev. Sci. Instrum.* **83**, 043107 (2012).
56. H. T. Lemke, M. Weaver, M. Chollet, J. Robinson, J. M. Glownia, D. Zhu, M. R. Bionta, M. Cammarata, M. Harmand, R. N. Coffee, D. M. Fritz, *SPIE Optics + Optoelectronics*, T. Tschentscher, K. Tiedtke, Eds. (SPIE, 2013), pp. 87780S–5.
57. M. Harmand, R. Coffee, M. R. Bionta, M. Chollet, D. French, D. Zhu, D. M. Fritz, H. T. Lemke, N. Medvedev, B. Ziaja, S. Toleikis, M. Cammarata, Achieving few-femtosecond time-sorting at hard x-ray free-electron lasers. *Nat. Photonics* **7**, 215–218 (2013).

Acknowledgments: We acknowledge E. Fradkin, S. A. Kivelson, T. Devereaux, B. Moritz, H. Jang, S. Lee, J.-S. Lee, C. C. Kao, J. Turner, G. Dakovski, and Y. Y. Peng for valuable discussions; D. Swetz for help during the experiments; and S. Zohar for support in data analysis. **Funding:** This work was supported by U.S. Department of Energy, Office of Basic Energy Sciences grant no. DE-FG02-06ER46285. The use of the LCLS, SLAC National Accelerator Laboratory was supported by DOE grant no. DE-AC02-76SF00515. The growth of LBCO single crystals was supported by DOE grant no. DE-SC0012704. M.M. acknowledges support from the Alexander von Humboldt Foundation, and P.A. acknowledges support from the Gordon and Betty Moore Foundation's EPiQS initiative through grant GBMF-4542.

Author contributions: M.M. and P.A. conceived the project. M.M., S.L., A.A.H., G.d.l.P.M., S.X.-L.S., Y.I.J., A.H.R., S.F.W., G.C., W.S., T.v.D., and P.A. conducted the experiment at the LCLS. M.M., S.L., A.A.H., G.d.l.P.M., and Y.I.J. analyzed the data with help from A.H.R. J.S. and G.D.G. synthesized the samples, and S.L. prepared them for the experiment. M.M., L.D., M.Z., S.H., N.G., and P.A. interpreted the results. M.M., N.G., and P.A. wrote the manuscript with input from all other authors. **Competing interests:** The authors declare that they have no competing interests. **Data and materials availability:** All data needed to evaluate the conclusions in the paper are present in the paper and/or the Supplementary Materials. Additional data related to this paper may be requested from the authors.

Submitted 14 March 2019
Accepted 3 July 2019
Published 16 August 2019
10.1126/sciadv.aax3346

Citation: M. Mitrano, S. Lee, A. A. Husain, L. Delacretaz, M. Zhu, G. de la Peña Munoz, S. X.-L. Sun, Y. I. Joe, A. H. Reid, S. F. Wandel, G. Coslovich, W. Schlotter, T. van Driel, J. Schneeloch, G. D. Gu, S. Hartnoll, N. Goldenfeld, P. Abbamonte, Ultrafast time-resolved x-ray scattering reveals diffusive charge order dynamics in $La_{2-x}Ba_xCuO_4$. *Sci. Adv.* **5**, eaax3346 (2019).

Science Advances

Ultrafast time-resolved x-ray scattering reveals diffusive charge order dynamics in $La_{2-x}Ba_xCuO_4$

Matteo Mitrano, Sangjun Lee, Ali A. Husain, Luca Delacretaz, Minhui Zhu, Gilberto de la Peña Munoz, Stella X.-L. Sun, Young Il Joe, Alexander H. Reid, Scott F. Wandel, Giacomo Coslovich, William Schlotter, Tim van Driel, John Schneeloch, G. D. Gu, Sean Hartnoll, Nigel Goldenfeld and Peter Abbamonte

Sci Adv **5** (8), eaax3346.
DOI: 10.1126/sciadv.aax3346

Science Advances
AAAS

advances.sciencemag.org/cgi/content/full/5/8/eaax3346/DC1

Supplementary Materials for

Ultrafast time-resolved x-ray scattering reveals diffusive charge order dynamics in $La_{2-x}Ba_xCuO_4$

Matteo Mitrano*, Sangjun Lee, Ali A. Husain, Luca Delacretaz, Minhui Zhu, Gilberto de la Peña Munoz, Stella X.-L. Sun, Young Il Joe, Alexander H. Reid, Scott F. Wandel, Giacomo Coslovich, William Schlotter, Tim van Driel, John Schneeloch, G. D. Gu, Sean Hartnoll, Nigel Goldenfeld*, Peter Abbamonte*

*Corresponding author. Email: mmitrano@illinois.edu (M.M.); nigel@illinois.edu (N.G.); abbamonte@mrl.illinois.edu (P.A.)

Published 16 August 2019, *Sci. Adv.* **5**, eaax3346 (2019)
DOI: 10.1126/sciadv.aax3346

This PDF file includes:

Supplementary text

Note S1. Pump-probe cross-correlation

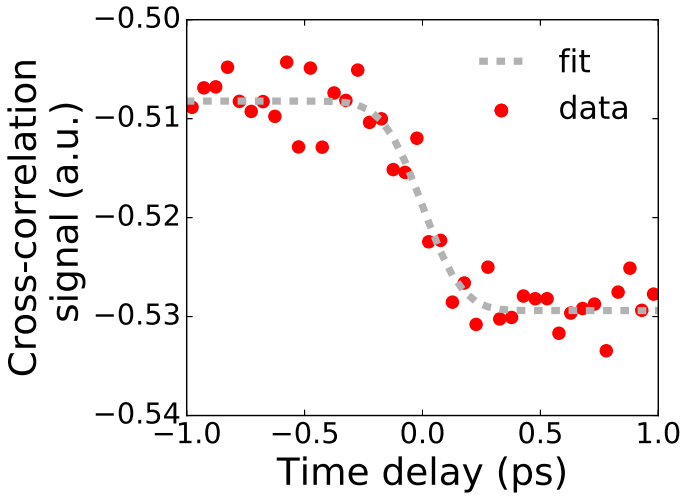

Fig. S1. Optical pump X-ray probe cross-correlation. Time-sorted YAG transmittance edge measuring the cross-correlation between optical pump and soft X-rays at the sample position. The signal intensity is uncorrected for amplitude fluctuations of the FEL beam. The fit function is given in the text.

The pump-probe cross-correlation for this experiment was measured by detecting the optical transmittance of the 1.55 eV light as a function of delay w.r.t the X-ray pulse for a 0.5 mm thick polished Ce:YAG placed at the sample position using a Si photodiode (model DET36A). When interacting with the X-ray beam, the YAG transmittance at 1.55 eV exhibits a sharp edge (see fig. S1) that can be used to characterize the global time resolution. By fitting the signal with the function $I(t) = I_0 - \frac{\Delta I}{2}[1 + \mathrm{erf}(\frac{t}{\tau_0})]$, we obtain a cross-correlation width $\tau_0 = (187 \pm 39)$ fs. Hence, our global time-resolution is $\tau_0/\sqrt{2} \sim 130$ fs under the assumption of Gaussian beam envelopes.

Note S2. Charge order peak rocking curves fit and background subtraction

The rocking curves shown in fig. S2 have been fitted with a pseudo-Voigt profile and a linear background,

$$I(q)\Big|_t = (I_0 + mq) + f\frac{1}{\pi g}\frac{A}{1+\left(\frac{q-Q_{CO}}{g}\right)^2} + (1-f)\frac{A}{g}\sqrt{\frac{\ln 2}{\pi}}\exp\Big[-\ln 2\Big(\frac{q-Q_{CO}}{g}\Big)^2\Big] \quad \text{(S1)}$$

The first term represents the linear background, while the second and third term represent a Lorentzian and a Gaussian, respectively, with f as a linear mixing parameter. The last two terms share the same amplitude parameter A and the same FWHM $2g$. The fit parameters at each time delay along the H direction (fig. S2) are reported in fig. S3. The background slope and intercept are constant over the entire delay window, therefore a background subtraction based on the fitted slope does not introduce artifacts in the time-dependent behavior of the charge-order (CO) peak. The fit parameters in fig. S3A to D exhibit a time dependence that can be captured by a single exponential recovery and an offset, while the background is time-independent. The same fit procedure has been also applied for the scans along the K direction shown in fig. S2B. The fit parameters for those curves are reported in Table S1.

Table S1. Fit parameters along K projection. Pseudo-Voigt fit parameters for the curves in fig. S2B. K_{CO} is the Miller index of the Q_{CO} wavevector in the fit expression.

	t<0.0 ps	t=1.0 ps
A (a.u.)	$(14.02 \pm 0.34) \cdot 10^{-3}$	$(6.35 \pm 0.28) \cdot 10^{-3}$
K_{CO}	$(0.0 \pm 0.3) \cdot 10^{-4}$	$(-7.4 \pm 0.5) \cdot 10^{-4}$
g (r.l.u.)	$(4.03 \pm 0.05) \cdot 10^{-3}$	$(5.23 \pm 0.09) \cdot 10^{-3}$
f	(0.655 ± 0.048)	(0.652 ± 0.080)
m (r.l.u.)	(0.00 ± 0.18)	(0.00 ± 0.10)
I_0 (a.u.)	(2.3031 ± 0.0057)	(2.3168 ± 0.0042)

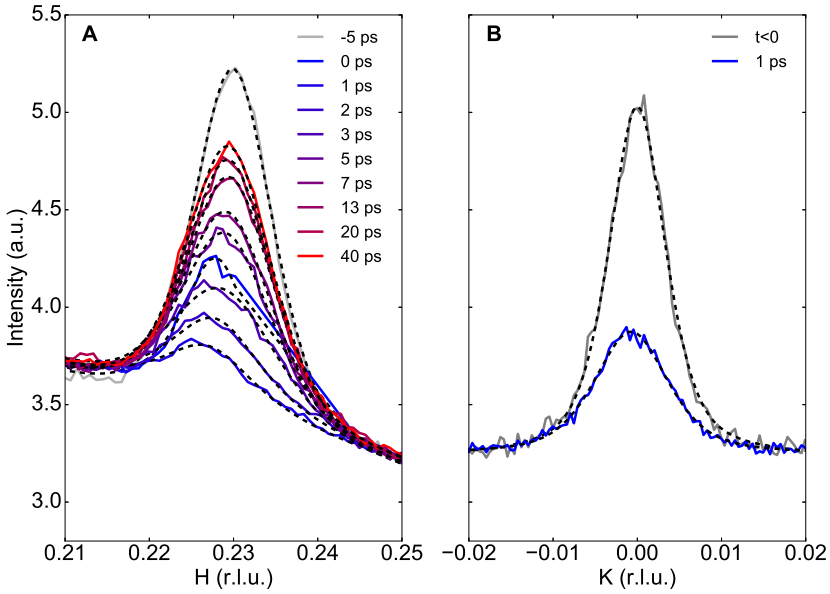

Fig. S2. Pump-induced CO peak melting. CO peak projection along H and K for selected time delays. Solid lines are experimental data, dashed lined represent pseudo-Voigt fits.

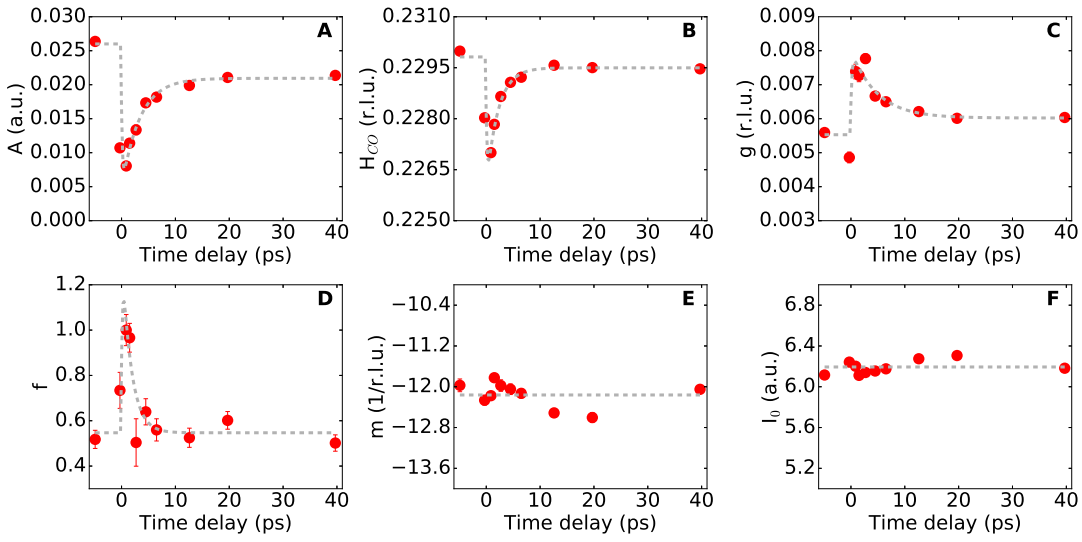

Fig. S3. Time-dependent CO peak fit parameters. (A) Pseudo-Voigt amplitude A, (B) H projection of the CO wavevector Q, (C) CO peak HWHM g, (D) Pseudo-Voigt mixing parameter f, (E) linear background slope m (F) linear background intercept I_0. Red symbols mark the fit parameters. These points are then fit to an exponential decay in (A)-(D) (dashed grey lines) and to a constant in (E)-(F).

Note S3. Charge order peak rocking curves for $\phi \sim \pi$

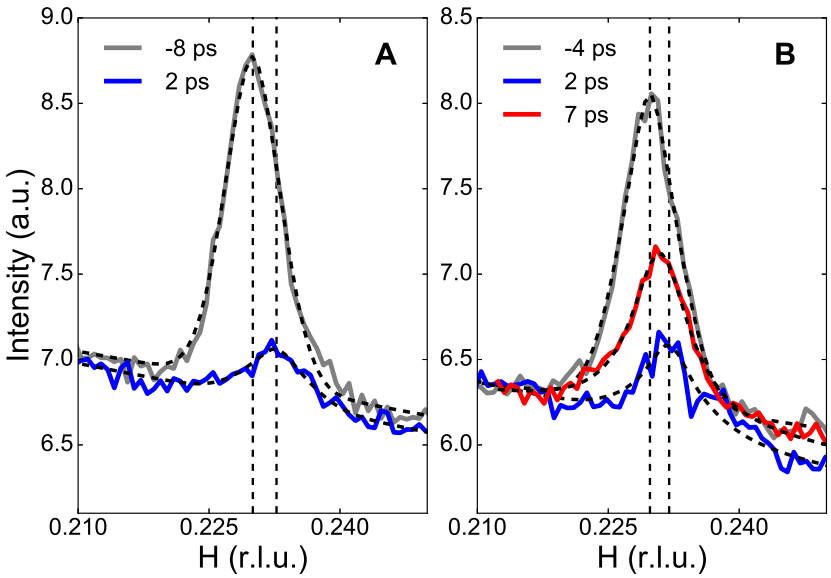

Fig. S4. CO peak shift at $\phi \sim \pi$. CO peak projection along H for selected time delays. Solid lines are experimental data, dashed lines represent pseudo-Voigt fits. Vertical dashed lines indicate the peak positions at equilibrium and at the maximum of the response. Data shown in (A) are acquired with a pump fluence of 0.2 mJ/cm^2 while data in (B) with 0.1 mJ/cm^2.

In the main text, we discuss the change in the CO peak shift direction when rotating the sample around the azimuthal angle ϕ. In fig. S4, we show the raw CO rocking curves for the blue points in Fig. 1B of the main text. These data are acquired at the same pump fluence and temperature conditions as the data reported in the rest of Fig. 1. Moreover, here we also report a second dataset exhibiting a clear peak shift when irradiated with a higher IR pump fluence.

Note S4. Comparison between tr-RIXS and APD data

The time-dependent elastic line intensity measured with the RIXS spectrometer and integrated over the energy axis maps closely onto the time-dependent, background-subtracted CO peak intensity measurement carried out with the avalanche photodiode (see fig. S5).

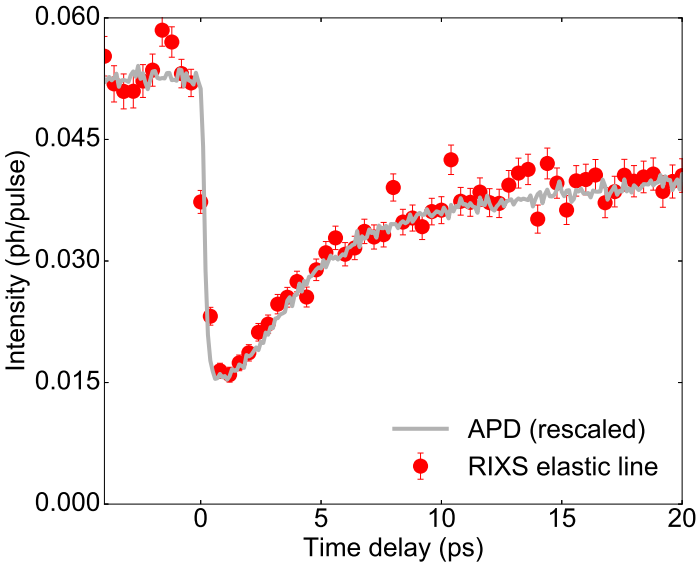

Fig. S5. Comparison between tr-RIXS and energy-integrated time dependence at Q_{CO}. Elastic line intensity values (energy-integrated in a 1.5-eV range around the peak) vs time delay are reported as red dots, while a rescaled, background-subtracted photodiode (APD) intensity measurement at Q_{CO} is shown as a solid grey line. Error bars are Poisson uncertainties.

Note S5. Response of the low-temperature tetragonal distortion peak

The onset of CO in 1/8-doped LBCO is accompanied by a low-temperature structural transition from a low-temperature orthorhombic (LTO) to a low-temperature tetragonal (LTT) phase (1). This structural change allows us to observe an otherwise forbidden (0,0,1) Bragg reflection. The (0,0,1) reflection measurement is performed at resonant condition with Cu L_3 edge X-rays. Previous studies reported pump-induced changes in this peak under 1.55 eV (*35*) and midinfrared (*34*) irradiation and for mJ/cm^2 fluences. Hence it is important to check whether

the structure responds as well to the excitation in the current experimental conditions. The (0,0,1) peak data at the same fluence of the CO data shown in the main text are shown in fig. S6. The peak intensity decreases but the peak does not shift in Q, at variance with the CO diffraction signal. This is additional evidence that the lattice does not change while the charge moves.

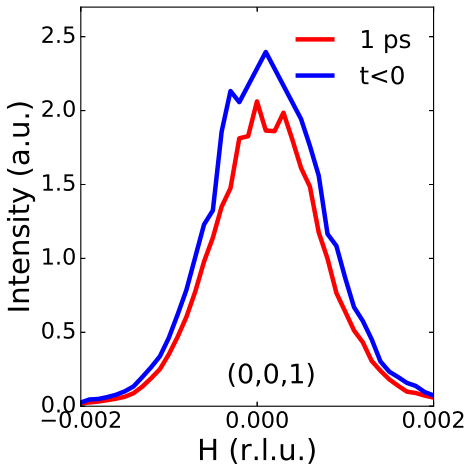

Fig. S6. Dynamics of the low-temperature tetragonal distortion. Projection of the (0,0,1) Bragg peak along the H direction at T=12 K for selected time delays and for a pump fluence of 0.1 mJ/cm^2.

Note S6. Raw time-dependent, energy-integrated peak intensities around Q_{CO}

In Fig. 3A of the main text, we show normalized differential intensity changes vs pump-probe time delay. In fig. S7 we show the unscaled intensity curves after time-sorting and rebinning with 200 fs time steps. Shot-to-shot intensity fluctuations have been corrected with a reference intensity monitor prior to the monochromator, while the fluorescence background has not been subtracted out. Each intensity curve is fit with a single exponential recovery and an offset capturing the long-time relaxation of the CO peak. The fit function for each momentum cut is

$$I(t)\Big|_q = \left|\Delta_0 - \Theta(t-t_d)\left[1-\exp\left(-\frac{t-t_d}{\tau_0}\right)\right]\left[A_0 + A_1\exp\left(-\frac{t-t_d}{\tau}\right)\right]\right|^2 + I_{\text{bkg}}. \quad \text{(S2)}$$

In this expression, the pump-induced signal grows with an exponential saturation characterized by a timescale τ_0. A_1 and A_0 respectively represent the exponential amplitude and an offset, while τ is the timescale of the exponential recovery. t_d is the parameter for the zero time delay. Δ_0 is the equilibrium value of the order parameter, while I_{bkg} is the fluorescence contribution to the overall intensity. The fit curves are indicated in fig. S7 as black dashed lines.

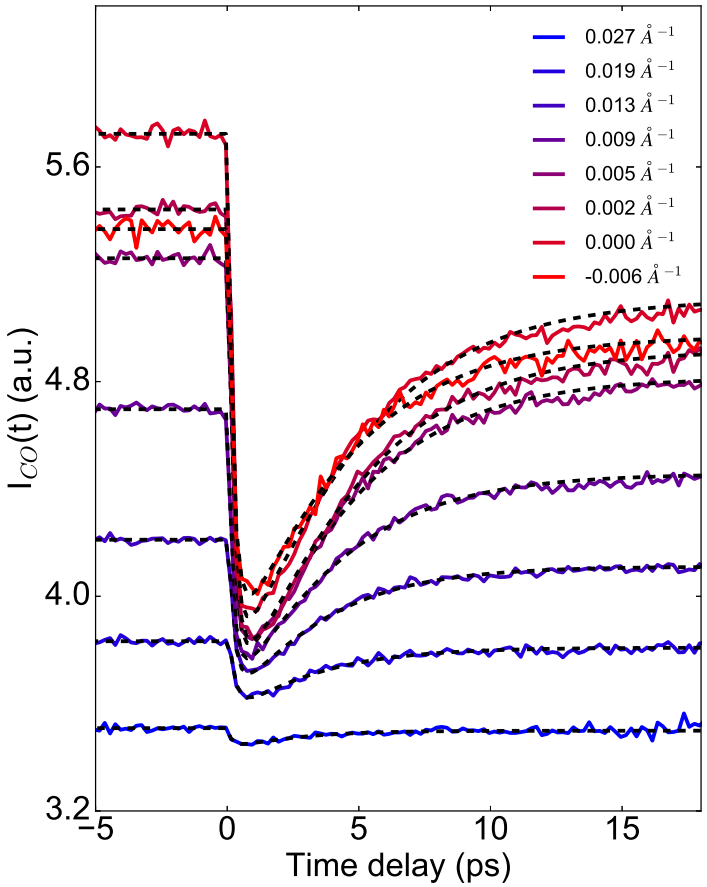

Fig. S7. Raw time-dependent CO peak intensity. Energy-integrated, time-dependent intensity profiles of the CO peak for a pump fluence of 0.1 mJ/cm^2 and for selected momenta (solid lines). Data are binned along the time axis in 200 fs steps to improve statistics. Single exponential fit curves are shown as dashed black lines.

Note S7. Momentum-dependent recovery of the charge-ordered phase

The purpose of this section is to calculate the relaxation of long-wavelength fluctuations of the charge order parameter as it approaches an equilibrium periodic state, in the spirit of Landau theory. The calculation remains in the framework of the time-dependent Ginzburg-Landau equation but the coarse-grained free energy takes into account the periodic charge order state.

Our data indicate that following the application of a laser pulse, the periodic state undergoes exponential relaxation with a rate $\gamma(\mathbf{q})$ in the interval 2 ps $< t <$ 10 ps, where $\mathbf{q}$ is the momentum relative to the charge order peak at $\mathbf{Q}_{CO}$. Our goal is to calculate the functional form of $\gamma(\mathbf{q})$, and show that it is of the form of Eq. (1) in the main text.

We model the charge density condensate as a function of space $\mathbf{x}$ and time t by the Swift-Hohenberg equation, a widely used minimal model of periodic pattern formation (*41,42*), which has previously been used to describe charge density wave dynamics (*43*). Written in canonical form it is

$$\tau_0 \frac{\partial \psi}{\partial t} = \epsilon\psi - \psi^3 - \xi_0^4 (q_0^2 + \nabla^2)^2 \psi \tag{S3}$$

Here $\psi = \psi(\mathbf{x}, t)$ is the charge order parameter rescaled so that the cubic term has coefficient unity, τ_0 is a relaxation time, q_0 is the magnitude of the wavevector at the onset of ordering when the control parameter $\epsilon > 0$ and ξ_0 is a charge fluctuation correlation length. The control parameter is determined by the degree to which the temperature is below the critical temperature for charge ordering. In the experiment, apart from the period when the system is excited by the laser, the temperature is well below the critical temperature, and we are deep into the regime where periodic charge order occurs. In principle this equation should have an additive noise that obeys the fluctuation-dissipation theorem, but this will not concern us if we restrict our calculation purely to linear stability. Note that the Swift-Hohenberg equation does not conserve the charge, and this is appropriate because it is only the total charge from the condensate and

the quasi-particles that is conserved.

When $\epsilon > 0$ the uniform state $\psi = 0$ becomes linearly unstable to the formation of a periodic state. The wavelength of this periodic state is not unique, because there is a band of linearly stable periodic steady states around the most unstable mode with wavenumber q_0, thus posing the so-called pattern selection problem. A large body of work shows in detail how the initial and boundary conditions as well as the history of the system determine which of these possible steady states is actually chosen by the dynamics (*42*), but here we simply use the observed charge order state rather than try to predict what it should be. Given that a periodic state of charge order exists, the next step is to perform the linear stability analysis around this pattern.

We assume the stripe patterns are periodic in the x direction, and constant in the y direction, and make a single-mode approximation

$$\psi(\mathbf{x}, t) = \psi_0 \left[A(x, y, t) e^{iq_0 x} + c.c. \right] \tag{S4}$$

where the slowly-varying complex amplitude A can be shown to obey the equation (*42*)

$$\partial_t A = \epsilon A + \mu_0^2 \left(\partial_x - \frac{i}{2q_0} \partial_y^2 \right)^2 A - 3|A|^2 A \tag{S5}$$

where $\mu_0 = 2q_0$. It is known that the single-mode approximation is qualitatively accurate and that the dependence with ϵ of the selected wave vector is weak, so we use this amplitude equation description as a first approximation to describe the long-wavelength dynamics.

Rescaling the equation by $q_0 \rightarrow \frac{q_0}{\mu_0}$, $A \rightarrow A/\sqrt{3}$ and $\mathbf{x} \rightarrow \mu_0 \mathbf{x}$, we obtain the Newell-Whitehead equation in canonical form (*44*)

$$\partial_t A = \epsilon A + \left(\partial_x - \frac{i}{2q_0} \partial_y^2 \right)^2 A - |A|^2 A \tag{S6}$$

Since the wavenumber of the stripes can be anywhere within the band, and is determined through an pattern selection process that is not of concern here, we will denote the wavenumber

of the actual selected stripe pattern to be $q_0 + k$. This means that our stability analysis is around the state described by the complex amplitude

$$A_k = a_k e^{ikx} \tag{S7}$$

where $a_k = \sqrt{\epsilon - k^2}$. We now impose a small perturbation, i.e. $A = A_k + \delta A$ with wavenumber $\mathbf{q} = (q_x, q_y)$ where

$$\delta A = (\delta a_+ e^{i\mathbf{q}\cdot\mathbf{x}} + \delta a_- e^{-i\mathbf{q}\cdot\mathbf{x}}) e^{ikx} \tag{S8}$$

and the negative mode is included due to the presence in the linearized equation of the term δA^*.

Plugging back into the Newell-Whitehead equation, we find the linearized equations of motion

$$\partial_t \delta a_+ = -(a_k^2 + U_+)\delta a_+ - a_k^2 \delta a_- \qquad \partial_t \delta a_- = -a_k^2 \delta a_+ - (a_k^2 + U_-)\delta a_- \tag{S9}$$

where

$$U_\pm = (k \pm q_x)^2 + \frac{(\pm q_x + k) q_y^2}{q_0} - \frac{q_y^4}{4q_0^2} - k^2 \tag{S10}$$

By writing eq. (S9) in matrix form and solving for the eigenvalues $\lambda_\pm$, we obtain:

$$\begin{aligned} \lambda_\pm &= -a_k^2 - \tfrac{U_+ + U_-}{2} \pm \sqrt{a_k^4 + \tfrac{(U_+ - U_-)^2}{4}} \\ &= -\epsilon + k^2 - q_x^2 - \tfrac{k q_y^2}{q_0} + \tfrac{q_y^4}{4q_0^2} \pm \sqrt{(\epsilon - k^2)^2 + 4k^2 q_x^2 + \tfrac{4k q_x^2 q_y^2}{q_0} + \tfrac{q_x^2 q_y^4}{q_0^2}} \\ &\simeq -\epsilon + k^2 - q_x^2 \pm \sqrt{(\epsilon - k^2)^2 + 4k^2 q_x^2} \\ &\simeq -\epsilon + k^2 - q_x^2 \pm \left[(\epsilon - k^2) + \tfrac{2k^2 q_x^2}{\epsilon - k^2}\right] \end{aligned} \tag{S11}$$

In the scattering geometry of our experiment, sketched in fig. S8, $q_y \ll q_x$ so that we find to a good approximation

$$\lambda_+ = -\frac{\epsilon - 3k^2}{\epsilon - k^2} q_x^2, \qquad \lambda_- = -2(\epsilon - k^2) - \frac{\epsilon + k^2}{\epsilon - k^2} q_x^2 \tag{S12}$$

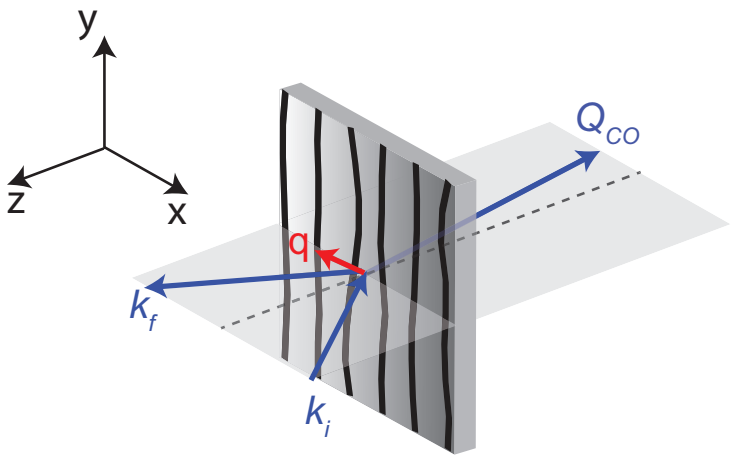

Fig. S8. Schematic representation of the scattering geometry. For the purpose of this section, the xy plane is defined as parallel to the CuO_2 planes. The scattering plane lies orthogonal to the stripe direction, here denoted as y. k_i and k_f represent the incident and scattered momenta of the x-ray beam, Q_{CO} is the charge order wavevector described in the main text and q is the small momentum deviation from Q_{CO} considered in this section.

The mode with eigenvalue λ_+ is a Goldstone phase mode that in the limit of vanishing q_x restores translational invariance. It is likely not to be present in our system because of disorder or grain boundaries between the stripe domains, both of which break translational invariance. The mode with eigenvalue λ_- is a decaying mode that corresponds to that measured in fig. 3B of the main text. We conclude by rewriting it in the physical units. The x-component of the measured charge order wavevector is $Q_{CO} = q_0 + k$ and $k \to k \cdot 2q_0 \cdot \xi_0^2$. Since **q** is defined relative to the charge order wavevector, we have that $q = q_x + O(q_y/q_x) \approx q_x$. Further neglecting the dependence of k on ϵ leads to the simple formulae for the decay rate extracted from the experiment

$$\gamma(q) = 2\epsilon + q^2 \tag{S13}$$

or in the original units

$$\gamma(q) = \frac{2\epsilon}{\tau_0} + \frac{(2q_0\xi_0^2)^2}{\tau_0} q^2 \tag{S14}$$

This result is Eq. (1) of the main text.